

MODELING OF CAPILLARY FORCES AND BINDING SITES FOR FLUIDIC SELF-ASSEMBLY

Karl F. Böhringer¹, Uthara Srinivasan^{2,3}, and Roger T. Howe^{2,4}

¹Electrical Engineering and Center for Applied Microtechnology
University of Washington, Seattle, WA 98195-2500

²Berkeley Sensor & Actuator Center, ³Chemical Engineering, ⁴Electrical Engineering and Computer Sciences
University of California, Berkeley, CA 94720-1774

ABSTRACT

Massively parallel self-assembly is emerging as an efficient, low-cost alternative to conventional pick-and-place assembly of microfabricated components. The fluidic self-assembly technique we have developed exploits hydrophobic-hydrophilic surface patterning and capillary forces of an adhesive liquid between binding sites to drive the assembly process. To achieve high alignment yield, the desired assembly configuration must be a (global) energy minimum, while other (local) energy minima corresponding to undesired configurations should be avoided. Thus, the design of an effective fluidic self-assembly system using this technique requires an understanding of the interfacial phenomena involved in capillary forces; improvement of its performance involves the global optimization of design parameters such as binding site shapes and surface chemistry.

This paper presents a model and computational tools for the efficient analysis and simulation of fluidic self-assembly. The strong, close range attractive forces that govern our fluidic self-assembly technique are approximated by a purely geometric model, which allows the application of efficient algorithms to predict system behavior. Various binding site designs are analyzed, and the results are compared with experimental observations. For a given binding site design, the model predicts the outcome of the self-assembly process by determining minimum energy configurations and detecting unwanted local minima, thus estimating expected yield. These results can be employed toward the design of more efficient self-assembly systems.

INTRODUCTION

The current “microengineering tool kit” consists of a wide range of methods including bulk and surface micromachining, laser micromachining, contact printing, and LIGA (German acronym for X-ray lithography, electrodeposition and molding). In the next generation of MEMS, micromechanical sensors and actuators will be integrated with electronic, optical, and fluidic components onto a variety of substrates to create powerful, complex microsystems [1]. Due to the materials incompatibility issues involved in monolithic integration, it seems that many of these applications will require efficient microassembly methods. Techniques developed to date are robotically-assisted pick-and-place assembly, and parallel assembly using wafer-to-wafer transfer or self-assembly of individual components (for a recent overview on microassembly see [2]).

As a wafer-scale assembly technique, self-assembly has two main advantages at the microscale: (1) it is highly economical since it matches the *parallel batch microfabrication techniques* with *parallel batch assembly*, and (2) it can be applied to *diverse*

microcomponent and substrate material combinations. Several research groups have demonstrated the self-assembly of microscale beads and microfabricated components onto a substrate using various forces for attraction and binding [3-8]. Recently, Srinivasan *et al.* have demonstrated a self-assembly technique at the microscale which relies upon capillary forces [9,10]. This technique is an extension of work done by Whitesides and coworkers at the milliscale [11,12], and Srinivasan and coworkers adapted it to self-assemble micromachined silicon parts onto silicon and quartz substrates with submicron positioning precision. This technique has been applied, *e.g.*, to position ultraflat micromirrors onto MEMS actuators [13].

With this technique, self-alignment occurs between matching binding site shapes coated with a hydrophobic self-assembled monolayer (SAM) and a meniscus of adhesive liquid between them (Fig. 1). While several site shapes have been tested [10], a systematic model of the self-assembly is needed in order to understand these results, as well as optimize binding site design for future work. In this paper, we address the issue of binding site design using a simple, yet accurate, model. We have demonstrated good agreement between the predicted behavior and experimental observations.

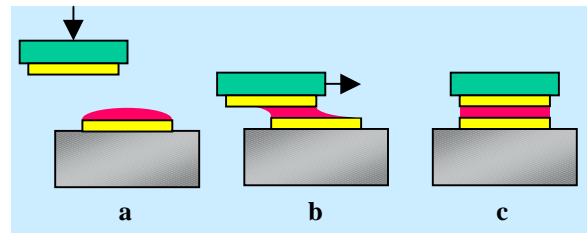


Figure 1. Schematic of fluidic self-assembly. Hydrophobic SAMs (bright) and adhesive (dark) result in self-alignment due to the capillary forces of the hydrophobic adhesive in water.

The paper is structured as follows. First, the experimental methods employed for this self-assembly technique are described. This motivates the modeling approach presented in the next section, which leads to the implementation of a simulator for fluidic self-assembly. Then, results from the simulations and experiments are presented and compared. A discussion of the findings, including the prediction of assembly states and self-assembly yield, follows. The paper concludes with a brief summary and directions for future work towards the automatic optimization of fluidic self-assembly systems.

EXPERIMENTAL METHODS

Our assembly technique is detailed in [9,10]. In this process, the binding sites are matching, hydrophobic shapes that need not

cover the entire surface of the part. In order to create these hydrophobic binding sites on the part and substrate surfaces, evaporated gold shapes are photolithographically patterned and self-assembled monolayers (SAMs) are deposited on them using alkanethiol precursor molecules. The gold regions are thereby rendered hydrophobic, while the remaining silicon or quartz areas are silicon dioxide-coated and hydrophilic. Then, the substrate is passed through a film of hydrophobic liquid adhesive on water, causing this hydrocarbon to selectively coat the binding sites since it does not wet the hydrophilic regions under water [14]. The microscopic parts are then directed towards the substrate surface under water using a pipette. Once the hydrophobic pattern on a part comes into contact with an adhesive-coated substrate binding site, the hydrocarbon liquid wets the part binding site and the restoring forces of the hydrocarbon capillary lead to self-alignment of the binding site on the part to that on the substrate. This occurs through interfacial free energy minimization of the adhesive-water and SAM-water interfaces. The assembled parts are held in place under water by the capillary forces of the adhesive, and permanent bonding is achieved by curing the adhesive using heat or ultraviolet light.

MODELING APPROACH

By definition, self-assembly is a spontaneous process that occurs in a statistical, non-guided fashion. More specifically, fluidic self-assembly is driven by the gradient in interfacial free energy when a part P approaches a substrate binding site S . An effective self-assembly system will exhibit a clear global energy minimum for the desired assembly configuration, while avoiding (as much as possible) local minima or regions of low energy gradient corresponding to undesired configurations in which the part could get stuck. Our goal is to model the interfacial energies during self-assembly, such that the system can be analyzed and its performance, yield, and shortcomings predicted.

We first derive a general expression for the change in surface energy during assembly of a part P onto a substrate S . For now we assume that P and S have rigid, flat surfaces. Before assembly, P and S are immersed in liquid, assumed here to be water. After assembly, P and S are in direct contact. Thus, the difference in free energy W can be written as

$$W = \gamma_{P,S} \cdot |P \cap S| + \gamma_{P,H_2O} \cdot |P - S| + \gamma_{S,H_2O} \cdot |S - P| - \left(\gamma_{P,H_2O} \cdot |P| + \gamma_{S,H_2O} \cdot |S| \right) \quad (1)$$

where $\gamma_{A,B}$ is the interfacial energy between surfaces A and B , and $|A|$ denotes the size of a surface A . The operators “ \cap ” and “ $-$ ” are geometric intersection and difference, respectively.

For our self-assembly purposes, the surfaces of P and S may not be homogeneous, but rather patterned into hydrophobic and hydrophilic regions. Let us denote the hydrophilic regions of P and S with P^+ and S^+ , respectively, and the hydrophobic regions with P^- and S^- (note that $P^+ \cup P^- = P$ and $S^+ \cup S^- = S$). Then we can write eq. (1) more detailed as

$$W = \sum_{P^+, P^-} \sum_{S^+, S^-} \gamma_{P_i, S_j} \cdot |P_i \cap S_j| + \sum_{P^+, P^-} \gamma_{P_i, H_2O} \cdot |P_i - S| + \sum_{S^+, S^-} \gamma_{S_j, H_2O} \cdot |S_j - P| - \left(\sum_{P^+, P^-} \gamma_{P_i, H_2O} \cdot |P_i| + \sum_{S^+, S^-} \gamma_{S_j, H_2O} \cdot |S_j| \right) \quad (2)$$

We observe that under these conditions, the free energy of assembling P and S is directly proportional to the respective contact areas of P and S , and the proportionality factor is given by the specific interfacial energy $\gamma_{A,B}$.

The interfacial energies between hydrophilic surfaces and water are small, *i.e.*, $\gamma_{A+, H_2O} \approx 0$. Further, $\gamma_{AA} \approx 0$ for all surfaces A . In contrast, interfaces between hydrophobic surfaces and water exhibit high surface energy, *i.e.*, $\gamma_{A-, H_2O} \gg 0$. Similarly, $\gamma_{A-A+} \gg 0$, and since in this application of fluidic self-assembly, hydrophilic surfaces will always retain a thin water film, we can assume that $\gamma_{A-A+} \approx \gamma_{A-, H_2O}$. Therefore, we can further simplify eq. (2) to

$$W = \gamma_{P^-, S^+} \cdot |P^- \cap S^+| + \gamma_{S^-, P^+} \cdot |S^- \cap P^+| + \gamma_{P^-, H_2O} \cdot |P^- - S| + \gamma_{S^-, H_2O} \cdot |S^- - P| - \left(\gamma_{P^-, H_2O} \cdot |P^-| + \gamma_{S^-, H_2O} \cdot |S^-| \right) = \gamma_{P^-, H_2O} \cdot |P^- - S^-| + \gamma_{S^-, H_2O} \cdot |S^- - P^-| - \left(\gamma_{P^-, H_2O} \cdot |P^-| + \gamma_{S^-, H_2O} \cdot |S^-| \right) = - \left(\gamma_{P^-, H_2O} + \gamma_{S^-, H_2O} \right) \cdot |P^- \cap S^-| \quad (3)$$

Eq. (3) states that the interfacial energy gain by assembling P and S is simply proportional to the overlap of the hydrophobic regions of P and S . If the same hydrophobic coatings are used for both P^- and S^- then eq. (3) becomes

$$W = -2\gamma_{\pm} \cdot |P^- \cap S^-| \quad (4)$$

where γ_{\pm} is the interfacial energy of all hydrophobic-hydrophilic interfaces. Table 1 summarizes the experimentally determined surface energies, as well as a literature value for $\gamma_{H_2O, \text{hexadecane}}$.

Interface	Interfacial Energy γ (mJ/m ²)
SAM - H ₂ O	≈ 46
SAM - SiO ₂	≈ 46
SAM - hexadecane	< 1
H ₂ O - hexadecane	52.2
H ₂ O - SiO ₂	< 1

Table 1. Interfacial energies of the surface materials used in fluidic self-assembly. Values were determined by contact angle measurements.

Interpretation of model: Eq. (4) states that the interfacial free energy of the self-assembly system is directly proportional to the hydrophobic surfaces exposed in aqueous environment. The energy of the system is lowered only when hydrophobic surfaces mate. This assumes that the interfacial forces act at very short range, such that all surface interactions are strictly locally. This is a good approximation of the situation when the adhesive layer present on a substrate binding site is very thin or non-existent.

Role of hydrophobic adhesive: The liquid adhesive droplets on the substrate binding sites drive the self-assembly process. These droplets serve three functions: (1) they generate the non-local capillary forces that pull the part binding site to match the substrate binding site, (2) they serve as lubricant coatings, facilitating motion of the part, and (3) they result in permanent bonding once the assembly is complete.

Limitations of model. If there is a substantial amount of adhesive on the binding sites, it can no longer be assumed that interaction between hydrophobic surface patches is strictly local. For example, the adhesive could form a “bridge” between hydrophobic areas P and S that do not immediately touch or overlap. In addition, the curved surfaces of the adhesive droplets can violate the assumption of a rigid, flat surface area. Therefore, the model is accurate only if the adhesive film thickness is small compared to the binding site size. In our experiments, typical values for the adhesive volume and thickness post-assembly were 0.28 nL and 8.9 μm , respectively, for a circular site of radius 100 μm .

IMPLEMENTATION

A software package was developed in MATLAB that implements the model described in the previous section. When the user enters specific designs for the hydrophobic regions P and S , the system can perform various computations related to the surface energetics of the system, thus allowing the user to characterize the self-assembly system and to predict its performance. The key functions are briefly described below. In general, P is assumed to be adjacent to S , and the configuration of P is given by the parameters x, y, θ , which describe the translation and rotation of P relative to S .

1. **Interfacial free energy of assembly:** For a given configuration (x, y, θ) , determine the interfacial free energy of the system.
2. **Energy minima for fixed orientation θ :** Determine all (x, y) coordinates of (local) energy minima.
3. **Global energy minima:** Determine the (x, y, θ) coordinates such that P is at a local or global energy minimum (corresponding to desired or undesired assembly states).

Since our model is based on the simple concept of geometric intersection of two arbitrary shapes, we can employ highly efficient numerical algorithms to perform the functions listed above. For example, the intersection $P \cap S$ for arbitrary (x, y) values and a fixed angle θ can be directly derived from the convolution of P

and S . Thus, operations (1) and (2) are performed essentially in a single MATLAB function call. Operation (3) requires one iteration over a range of θ values.

RESULTS

A number of self-assembly experiments were performed with a variety of part and binding site shapes. The dimensions of the binding sites are given in Table 2, and the results of these experiments are summarized in Table 3. Further details on these experiments can be found in [10].

Binding Site Shape	Binding Site Dimensions	Part Dimensions
	$d = 100, 195 \mu\text{m}$	$d = 200 \mu\text{m}$
	$d = 200 \mu\text{m}$	$d = 500 \mu\text{m}$
	$l = 20, 40, 150 \mu\text{m}$	$l = 150 \mu\text{m}$
	$l = 380, 400 \mu\text{m}$	$l = 400 \mu\text{m}$
	$l = 500 \mu\text{m}$ $w = 250 \mu\text{m}$	$l = 500 \mu\text{m}$ $w = 250 \mu\text{m}$
	$d = 300 \mu\text{m}$	square, $l = 400 \mu\text{m}$
	$l = 327 \mu\text{m}$ $w = 253.5 \mu\text{m}$	square, $l = 400 \mu\text{m}$
	width = 20, 33 μm $d = 200 \mu\text{m}$	$d = 200 \mu\text{m}$

Table 2. Shapes and dimensions of binding site and test parts used in fluidic self-assembly experiments. Unless otherwise specified, parts have matching binding sites.

Parts	Yield (%)
Circles, squares, hexagons	100 (hundreds of parts)
Rectangles	15/15
Thick rings on thick rings	10/19
Circles on thick rings	20/27*
Thick rings on circles	30/30
Commas	3/12
Semicircles	4/12

Table 2. Observed yield in self-assembly experiments.
* Lower than expected yield due to incomplete wetting of the hydrophobic surfaces (see Discussion section).

In the remainder of this section we apply the model to several self-assembly systems, and compare the simulated outcomes with the results obtained in physical experiments.

Circles on Circles. Fig. 2 plots the surface energy for a circular binding site as described in Table 1 (row 1). The x and y axes represent the translation of the part relative to the substrate.

The vertical axis displays the negated interfacial free energy $-W$. The single, sharp peak at $(0,0)$ indicates that there exists only one global minimum for W . This minimum corresponds to an exact match between part and substrate binding site.

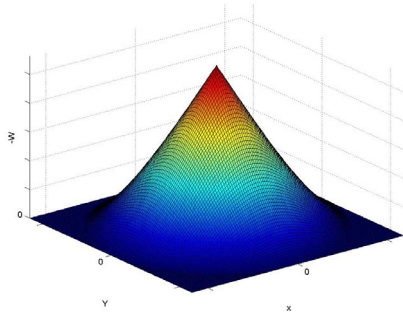


Figure 2. Surface energy of circular part and binding site as function of x and y position. The plot indicates a unique energy minimum at $(0,0)$ and a smooth transition to assembly without local minima, which is necessary for high yield self-assembly.

Perfect yield was observed for self-assembly with circular binding sites, for arrays with hundreds of elements. Note that circular parts only require alignment in x and y direction, while the orientation of the part is arbitrary.

Hexagons, Squares, or Rectangles. Regular polygons and convex designs with matching polygons behave similar to circles and exhibit high yield in assembly. Part symmetry induces multiple possible assembly orientations (hexagon: 6, square: 4, rectangle: 2 orientations).

Rings on Rings: In this experiment, the hydrophobic binding sites are in the shape of an open ring (the opening was introduced so that the adhesive could de-wet from the inside of the ring). Fig. 3a shows two incorrectly and two correctly assembled disks for this case. This design introduced local energy minima. These minima are predicted accurately by the modeling software (Fig. 3b). Fig. 4 shows the surface energies as a function of x and y position of P . A circular region of local maxima can be observed surrounding the central global maximum.

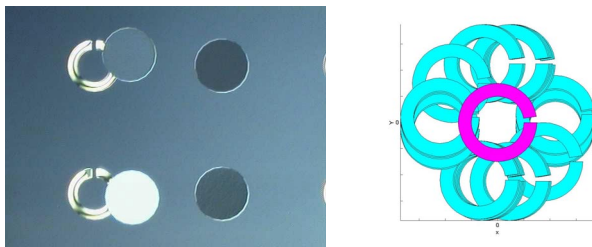


Figure 3. (a) Self-assembly of four Si disks with ring-shaped SAM pattern (on back side of parts) to ring-shaped binding sites on a Si substrate. Left: failed assemblies stuck at local energy minima. Right: successful assemblies. (b) Undesired assembly states corresponding to local energy minima as predicted by the modeling software (substrate binding site: dark; parts: bright). The discrete, non-evenly spaced configurations are due to discretization in the software.

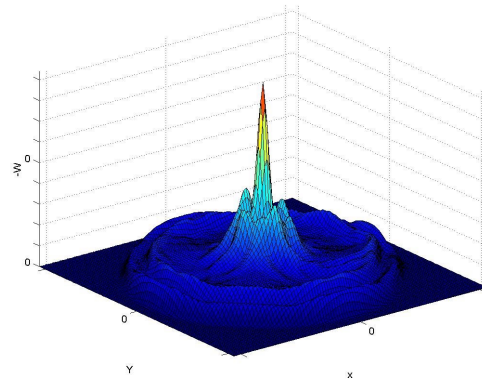


Figure 4. Interfacial free energy for self-assembly with the parts from Fig. 3, plotted (negated) as function of disk position. A large peak corresponding to the correct assembly state can be seen above $(0,0)$. But a region with local extrema can also be seen which corresponds to the incorrect assemblies in the left of Figure 2. Note: θ is not shown here since the ring design is rotationally symmetric.

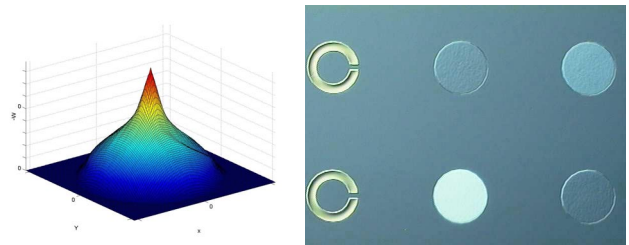


Figure 5. (a) Interfacial energy plotted (negated) for improved design using circular sites on the parts and open ring-shaped sites on the substrate. Only one global peak exists above $(0,0)$, corresponding to the correct assembly state. (b) Left: open ring-shaped binding sites. Right: Parts successfully assembled to the ring sites.

These local minima can be avoided by replacing the ring pattern on the part P with a disk. Fig. 5 shows the energy plot with the unique minimum, and a photograph of a successful assembly experiment.

The previous examples used rotationally symmetric designs. This simplified the analysis since the part orientation θ did not need to be taken into account. However, most binding sites will not exhibit this kind of symmetry. Rectangular sites as described in Table 2 (row 4) always give rise to two equivalent minima. For applications where the orientation is important (e.g., for the assembly of diodes) it would be desirable to obtain one unique minimum.

Comma-shaped sites: This shape represents an attempt to avoid duplicate minima by eliminating symmetry of the binding site. However, besides the correct assembly we also observe an incorrect assembly, which corresponds to a local minimum in the surface energetics, as can be seen in Fig 6. Fig. 7 shows the plot of the energy minima as a function of orientation θ . A second, lower peak can be seen at approximately 190 degrees, in good accordance with the experimental observation in Fig 6b.

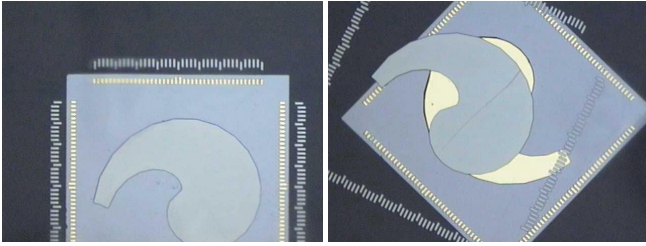


Figure 6. Self-assembly of square Si micropart with comma-shaped part and substrate binding site. Picture taken through underside of quartz substrate. (a) Correct assembly with micron-scale alignment. (b) Incorrect assembly at a local energy minimum.

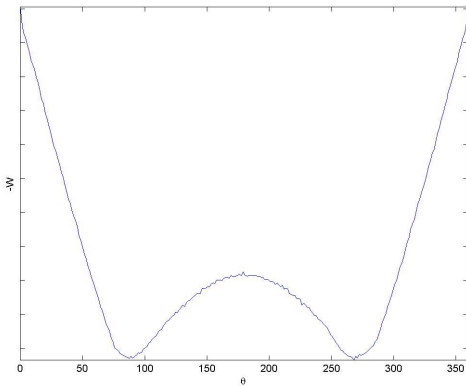


Figure 7. Interfacial energy W for the comma-shaped part plotted (negated) as function of θ . For each orientation θ the software minimizes the energy over the range of (x,y) positions. Two peaks can be seen here: the correct assembly for $\theta=0^\circ$ corresponding to Fig. 6a, and the incorrect assembly at about $\theta=190^\circ$ corresponding to Fig. 6b. Alignment yield is dependent on the ratio of the peak heights.

Binding Site from Three-Dimensional Self-Assembly: Gracias *et al.* [15] describe a self-assembling three-dimensional network made of millimeter-scale polyhedra with embedded electric components. Their binding site design is shown in Fig. 8a. We analyzed this design with our modeling software. Fig. 8b shows the interfacial energy plot for two patterns with relative rotation $\theta=0^\circ$. A clear peak can be observed for $(x,y)=(0,0)$. Minor local minima exist but are relatively small. Further analysis reveals the interesting property that for any given part orientation θ , the state of lowest energy is at $(0,0,\theta)$. This means that during self-assembly, the part will always be attracted to the position where the centers of the binding sites match, independent of the initial orientation of the part.

Fig. 9 shows the interfacial energy of the system as a function of rotation θ . The four-fold symmetry is immediately visible, as is the smooth shape without local minima or plateaus. We believe that the successful self-assembly experiments reported in [15] can be at least partially explained with this analysis.

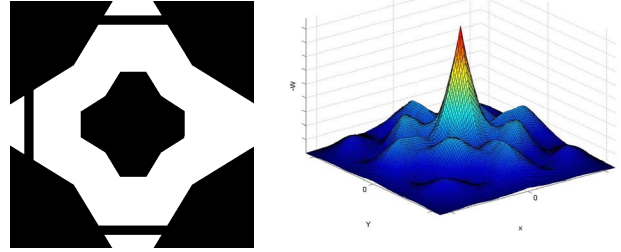


Figure 8. (a) Binding site design used for three-dimensional self-assembly by Gracias *et al.* [15]. (b) Surface energy plot (negated) for the binding site in (a) at rotation $\theta=0^\circ$ degrees.

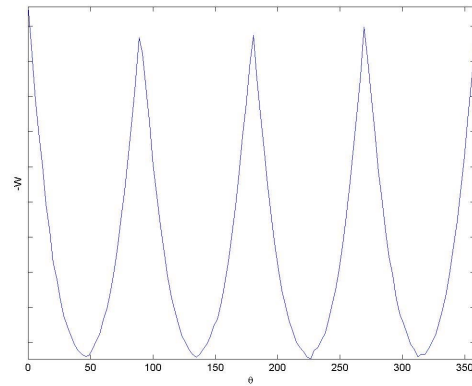


Figure 9. Minimum surface energy (negated) as function of part orientation θ for the binding site in Fig. 8. The four-fold symmetry of the site design is reflected in the 90° periodicity of the graph.

DISCUSSION

In general, good accordance was observed between predicted and experimental self-assembly performance. However, as described above, the model becomes less accurate if the meniscus of hydrophobic liquid between mating binding sites differs in shape substantially from the binding site design. This can occur when the volume of adhesive per site is too large or too small. For example, lower than expected self-assembly yield was observed for circles on rings (Table 2, row 7). Inspection of the assembly sites indicated that the adhesive was pulled off the ring-shaped binding site to the disk by capillary forces (Fig. 10).

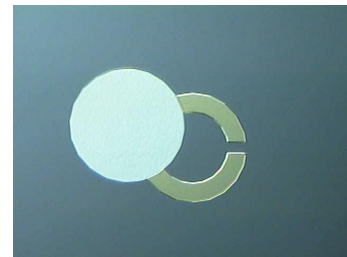


Figure 10. Close-up of a misaligned disk on a ring binding site. No adhesive is visible on the ring and is assumed to be concentrated under the disk.

The software uses efficient algorithms and can handle arbitrary binding site designs. The analysis of energy minima for a fixed angle of rotation θ as shown in Figs. 2, 3b, 4, 5a, and 8b is accomplished in a few milliseconds on a 500MHz Pentium II PC platform. The general analysis for the full range of configurations (x, y, θ) that leads to Figs. 7 and 9 is achieved in the order of seconds.

CONCLUSIONS AND FUTURE WORK

We have developed a model and computational tools for the efficient analysis and simulation of fluidic self-assembly systems. The performance of the software has been demonstrated on several sample experiments and observed good accordance between predicted and observed system behavior.

We are currently using the public domain finite element program *Surface Evolver* [16] to investigate the behavior of the liquid meniscus during self-assembly. Given the surface energy parameters of the liquid and the hydrophobic binding sites, *Surface Evolver* uses energy minimization to calculate the equilibrium shape of the liquid droplet. This model will aid in understanding the detailed dynamics of the self-assembly and in evaluating the capabilities and limitations of our model.

Currently, the model described in this paper is used to *analyze* given designs of fluidic self-assembly systems. In the next stage of the project, the software can be extended to *automatically design and optimize* binding site shapes. The simplicity of the current model and its efficient implementation forms the basis to attack the complex and computationally more expensive task of design automation.

The software package is available upon request from K. Böhringer, karl@ee.washington.edu.

ACKNOWLEDGEMENTS

Research at the University of Washington was supported in part by NSF Career Award ECS-9875367 to K. Böhringer and by donations from Agilent Technologies, Intel Corporation, Microsoft Research, and Tanner Research Inc. Work at the University of California at Berkeley has been supported by the Berkeley Sensor & Actuator Center. We would also like to thank the staff of the Berkeley Microfabrication Facility for their helpful advice and support.

REFERENCES

1. M. B. Cohn, K. F. Böhringer, J. M. Noworolski, A. Singh, C. G. Keller, K. Y. Goldberg, and R. T. Howe, "Microassembly Technologies for MEMS," Proc. *SPIE Micromachining and Microfabrication*, Santa Clara, CA, USA, Sept. 20-22, 1998, pp. 2-16.
2. K. F. Böhringer, R. S. Fearing, and K. Y. Goldberg, "Microassembly," in *The Handbook of Industrial Robotics*, 2nd ed., John Wiley & Sons (1999), pp. 1045-1066.
3. H.-J. J. Yeh and J. S. Smith, "Fluidic Assembly for the Integration of GaAs Light-Emitting Diodes on Si Substrates," *IEEE Photonics Technology Letters*, 6, pp. 706-8 (1994).

4. T. Nakakubo and I. Shimoyama, "Three-Dimensional Micro Self-Assembly Using Bridging Flocculation," Proc. *Transducers '99 - Int. Conf. on Solid-State Sensors and Actuators*, Sendai, Japan, June 7-10, 1999, pp. 1166-9.
5. Y. Murakami, K. Idegami, H. Nagai, A. Yamamura, K. Yokoyama, and E. Tamiya, "Random Fluidic Self-Assembly of Microfabricated Metal Particles," Proc. *Transducers '99 - Int. Conf. on Solid-State Sensors and Actuators*, Sendai, Japan, June 7-10, 1999, pp. 1108-11.
6. M. Cohn, *Assembly Techniques for Microelectromechanical Systems*, Ph.D. dissertation, University of California at Berkeley, 1997.
7. K. L. Michael, L. C. Taylor, S. L. Schultz, and D. R. Walt, "Randomly Ordered Addressable High-Density Optical Sensor Arrays," *Analytical Chemistry*, 70, 1242-8 (1998).
8. X. Xiong, W. Wang, D. T. Schwartz, K.-F. Böhringer, "Controlled Self-Assembly of MEMS via Electrochemical Modulation of Interfacial Energetics." American Institute of Chemical Engineers (AIChE) Annual Meeting, Los Angeles, CA, November 12-17, 2000.
9. U. Srinivasan, R. T. Howe, and D. Liepmann, "Fluidic Microassembly Using Patterned Self-Assembled Monolayers and Shape Matching," Proc. *Transducers '99 - Int. Conf. on Solid-State Sensors and Actuators*, Sendai, Japan, June 7-10, 1999, pp. 1170-3.
10. U. Srinivasan, R. T. Howe, and D. Liepmann, "Microstructure to Substrate Self-Assembly Using Capillary Forces," *Journal of Microelectromechanical Systems*, accepted for publication July 2000.
11. A. Terfort, N. Bowden, and G. M. Whitesides. "Three-Dimensional Self-Assembly of Millimetre-Scale Components," *Nature*, 386, 162-4 (1997).
12. J. Tien, T. L. Breen, and G. M. Whitesides, "Crystallization of Millimeter-Scale Objects With Use of Capillary Forces," *J. American Chemical Society*, 120, 12670-1 (1998).
13. U. Srinivasan, M. H. Helmbrecht, C. Rembe, R. S. Muller, and R. T. Howe, "Fluidic Self-Assembly of Micromirrors onto Surface Micromachined Actuators," Proc. *2000 IEEE/LEOS Intl. Conf. on Optical MEMS*, Kauai, HI, USA, Aug. 21-4, 2000, pp. 59-60.
14. H. A. Biebuyck and G. M. Whitesides, "Self-Organization of Organic Liquids on Patterned Self-Assembled Monolayers of Alkanethiolates on Gold," *Langmuir*, 10, 2790-3 (1994).
15. D. H. Gracias, J. Tien, T. L. Breen, C. Hsu, G. M. Whitesides, "Forming Electrical Networks in Three Dimension by Self-Assembly," *Science*, 289, 1170-2 (2000).
16. *Surface Evolver* is available at www.susqu.edu/facstaff/b/brakke/evolver.html.